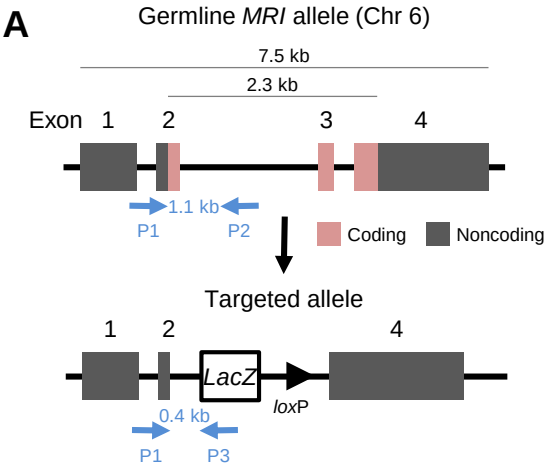

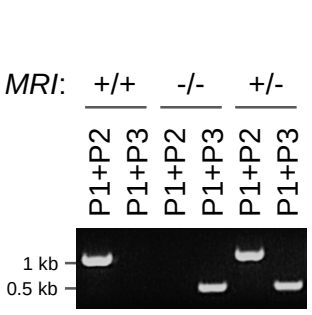

C

MRI	Expected	Actual
+/+	40	41
+/-	80	84
-/-	40	35
Total		**160**

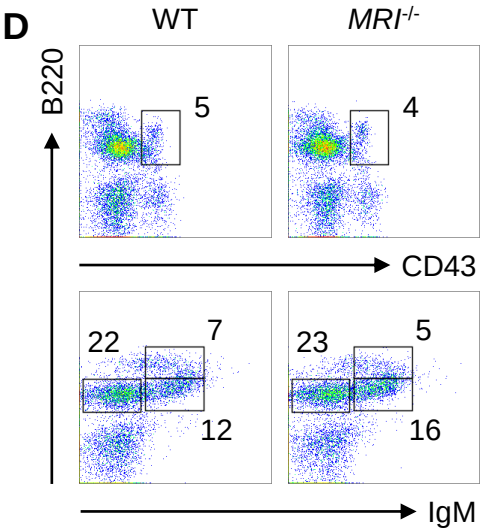

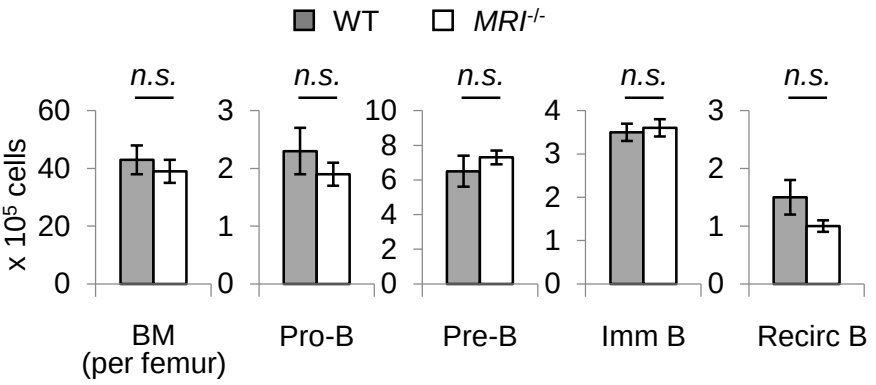

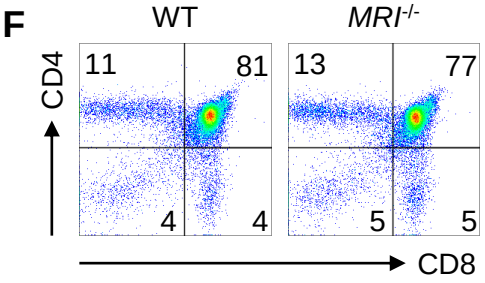

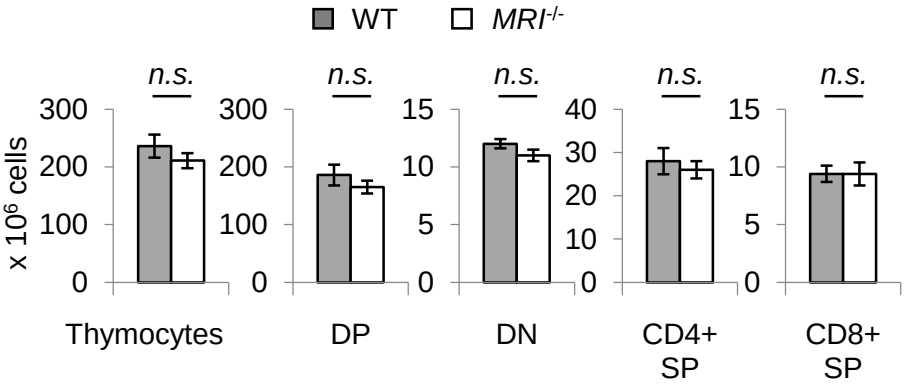

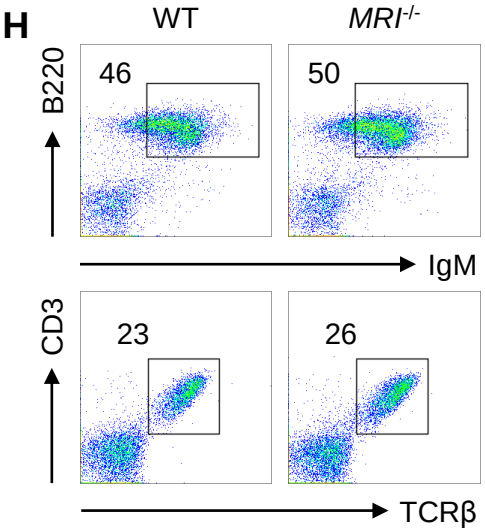

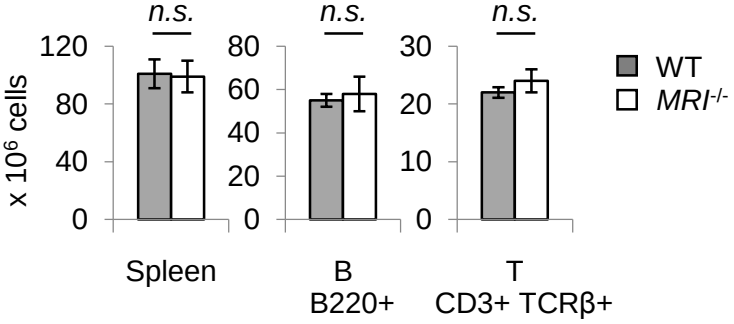

Figure S1, related to Figure 1. Lymphocyte development in *MRI*$^{-/-}$ mice. (A) Schematic of the murine *MRI* gene (top) and the targeted allele in which the entire protein-coding region is replaced by a *LacZ* cDNA cassette (bottom). Coding and non-coding regions of the gene are represented as pink and gray boxes, respectively. Primers used for genotyping are depicted as blue arrows (P1, P2, and P3). **(B)** PCR analyses of genomic DNA from *MRI*$^{+/+}$, *MRI*$^{-/-}$, and *MRI*$^{+/-}$ mice using the indicated primer pairs. **(C)** Numbers of live births produced from intercrossing *MRI*$^{+/-}$ mice. **(D)** Flow cytometric analyses of pro-B (B220+ CD43+ IgM-), pre-B (B220+ CD43- IgM-), immature B (B220^{low} CD43- IgM+), and recirculating mature B (B220^{high} CD43- IgM+) cells in the bone marrow (BM) of 6-week old WT and *MRI*$^{-/-}$ littermates. The percentage of cells in each gate is indicated. **(E)** Quantification of total BM, pro-B, pre-B, immature B, and recirculating B cells per femur. **(F)** Flow cytometric analyses of DP (CD4+ CD8+), DN (CD4- CD8-), and SP (CD4+ CD8- or CD4- CD8+) thymocytes in 6-week old WT and *MRI*$^{-/-}$ mice. The percentage of cells in each quadrant is indicated. **(G)** Quantification of total, DP, DN, CD4+ SP, and CD8+ SP thymocytes. **(H)** Flow cytometric analyses of mature B (B220+ IgM+) and T (CD3+ TCRβ+) cells in the spleens of 6-week old WT and *MRI*$^{-/-}$ mice. **(I)** Quantification of mature B and T cells in the spleen. All data are mean ± SEM (*n* = 5).

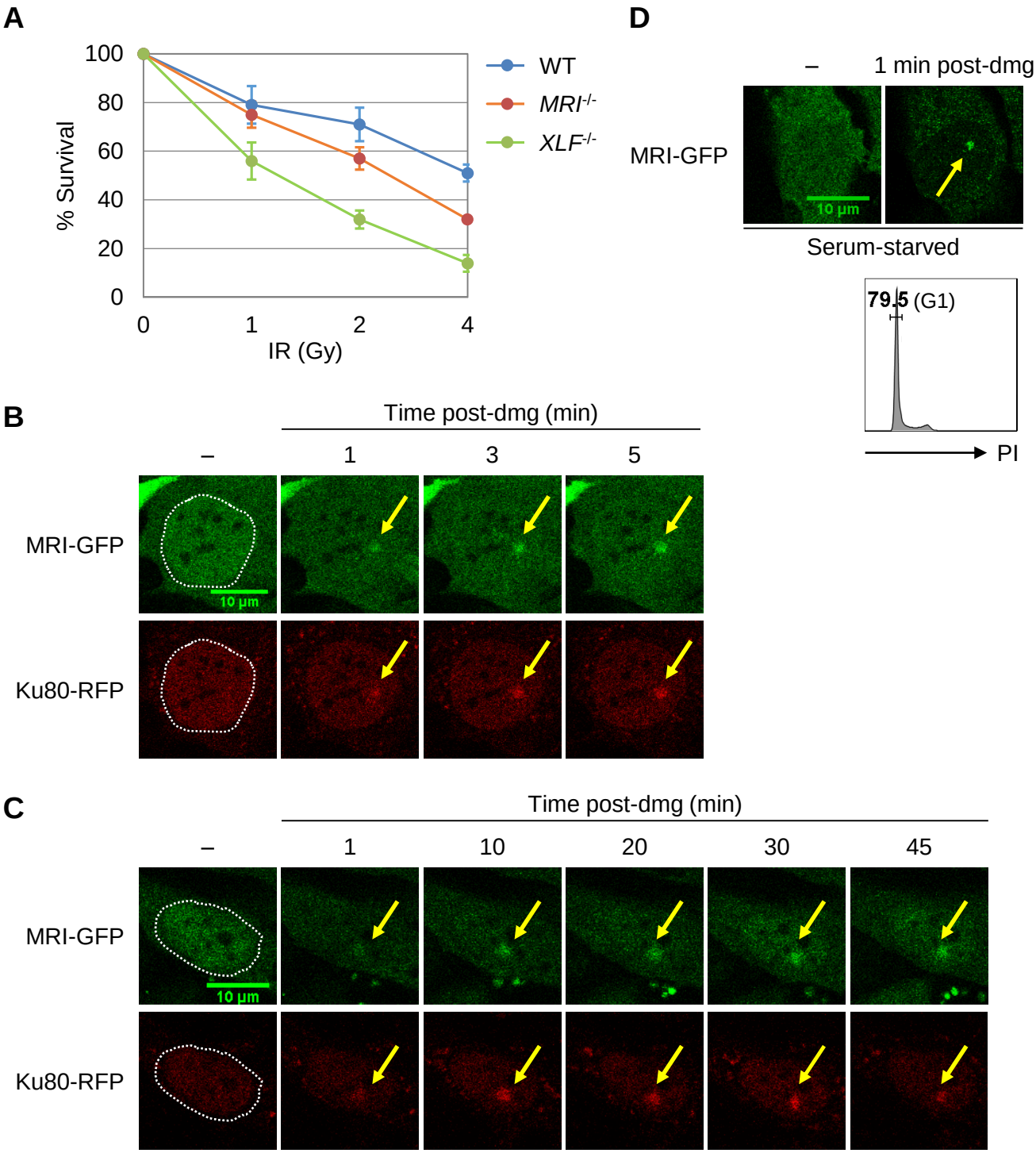

Figure S2, related to Figure 1. MRI functions in cNHEJ. (A) Percent survival of WT (line WT-1), *MRI*$^{-/-}$ (line M61.7), and *XLF*$^{-/-}$ (line X-AB) MEFs four days after exposure to the indicated doses of IR. Data are mean ± SEM (*n* = 3). These cell-lines were generated from different mice than the ones shown in Figure 1B. **(B and C)** Representative time-lapse micrographs of MRI-GFP and Ku80-RFP recruitment to a site of laser-induced DNA damage (designated by a yellow arrow) in *MRI*$^{-/-}$ MEFs at the indicated times post-damage (minutes, min). The dotted lines mark the nuclear boundaries. **(D)** Time-lapse micrographs of MRI-GFP localization to a site of laser-induced DNA damage in serum-starved *MRI*$^{-/-}$ MEFs (top). Flow cytometric analyses of cell cycle phase, as indicated by DNA content (propidium iodide, PI), in serum-starved MEFs (bottom).

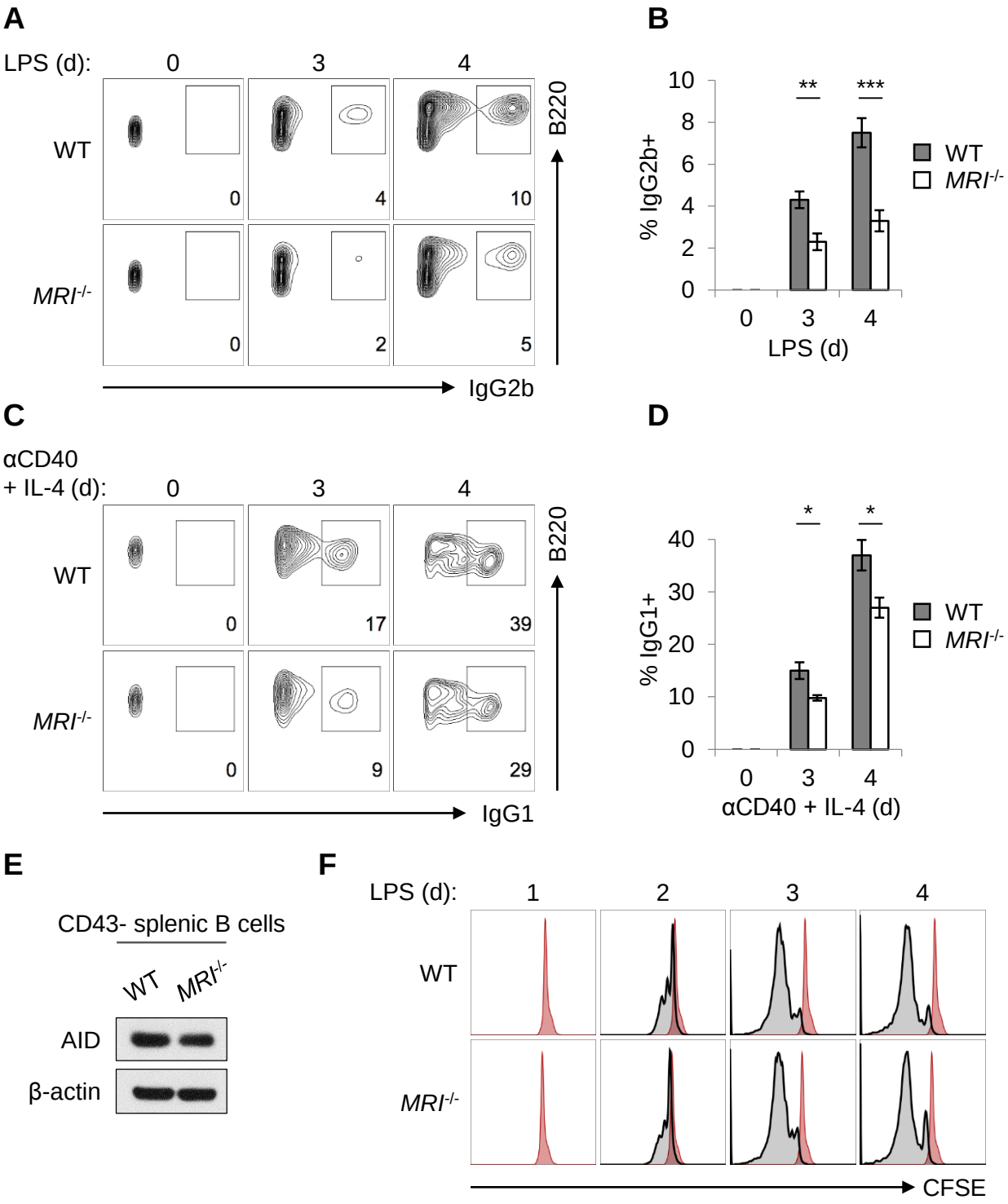

Figure S3, related to Figure 1. *MRI*$^{-/-}$ B cells exhibit an Ig CSR defect. (A) Flow cytometric analyses of IgG2b class-switching in WT and *MRI*$^{-/-}$ CD43- splenic B cells stimulated with LPS for three to four days (d). **(B)** Quantification of IgG2b+ cells after stimulation with LPS for the indicated lengths of time. Data are mean ± SEM (n = 6). * p <0.05, ** p <0.01, *** p <0.005. **(C)** Flow cytometric analyses of IgG1 class-switching in WT and *MRI*$^{-/-}$ CD43- splenic B cells stimulated with anti-CD40 and interleukin-4 (IL-4) for three to four days. **(D)** Quantification of IgG1+ cells after stimulation with anti-CD40 and IL-4 for the indicated lengths of time (n = 4). **(E)** Western blot analyses of AID in WT and *MRI*$^{-/-}$ B cells after stimulation with LPS for four days. β-actin is shown as a protein loading control. **(F)** Flow cytometric analyses of CFSE dilution in WT and *MRI*$^{-/-}$ B cells that were stimulated with LPS for the indicated lengths of time. The Day 1 histogram (red) is shown at each time point as a reference.

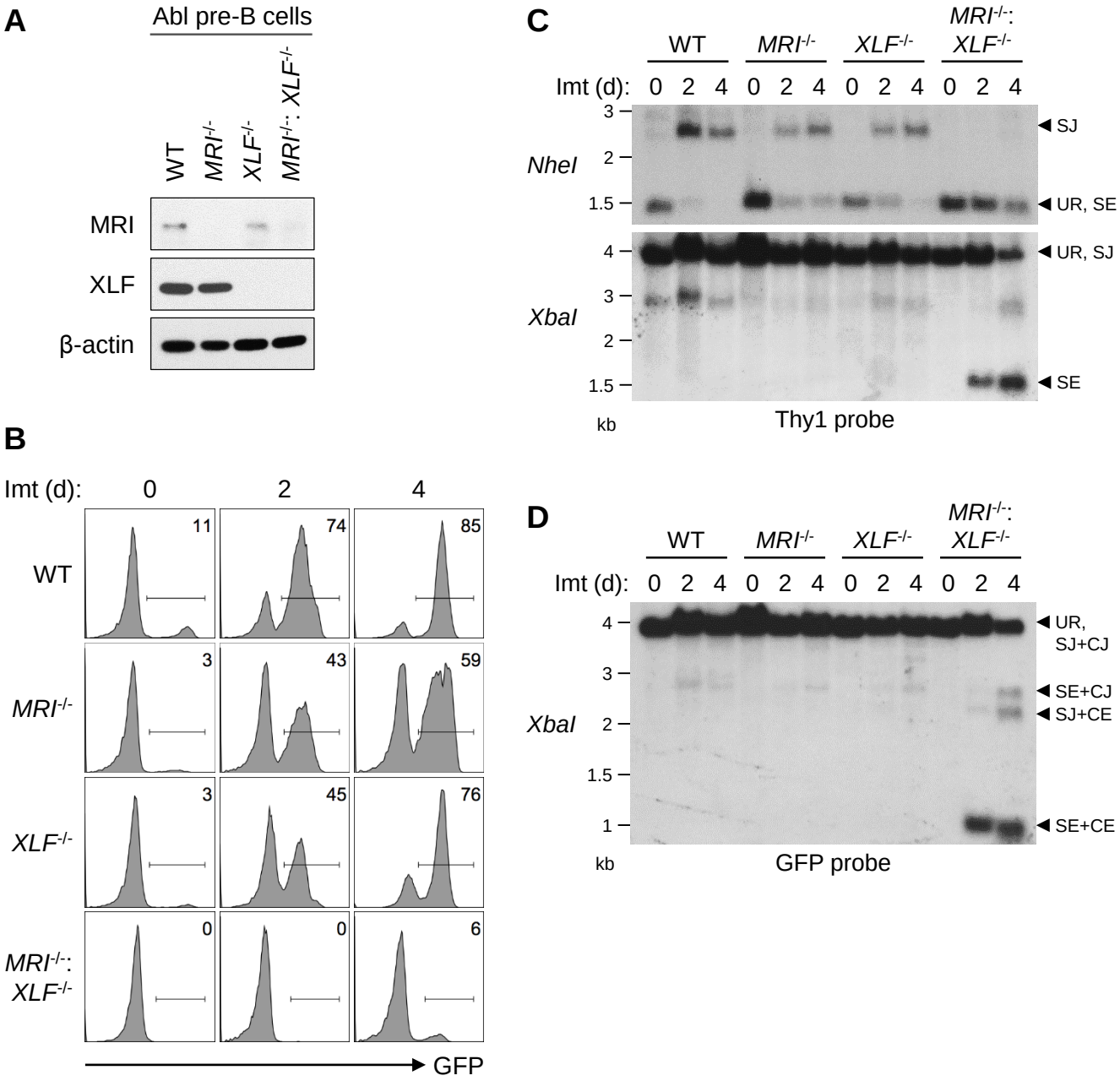

Figure S4, related to Figure 3. Combined MRI and XLF deficiency blocks cNHEJ-mediated repair of RAG DSBs. (A) Western blot analyses of MRI and XLF in WT, *MRI*$^{-/-}$, *XLF*$^{-/-}$, and *MRI*$^{-/-}$:*XLF*$^{-/-}$ abl pre-B cells. β-actin is shown as a protein loading control. **(B)** Flow cytometric analyses of GFP expression in WT (line M63.1-7), *MRI*$^{-/-}$ (line M46.3-19), *XLF*$^{-/-}$ (line XB1-5), and *MRI*$^{-/-}$:*XLF*$^{-/-}$ (line MX-4) abl pre-B cells that were treated with imatinib for the indicated lengths of time (days, d). These cell-lines are independent clones from the ones shown in Figure 3. **(C)** Southern blot analyses of genomic DNA from cells in (B) that were digested with *NheI* (top) or *XbaI* (bottom) and hybridized to the Thy1 probe. **(D)** Southern blot analyses of genomic DNA from cells in (B) that were digested with *XbaI* and hybridized to the GFP probe. Bands corresponding to different pMG-INV arrangements are indicated as described in Figure 3. Molecular weights (kilobases, kb) are also shown.

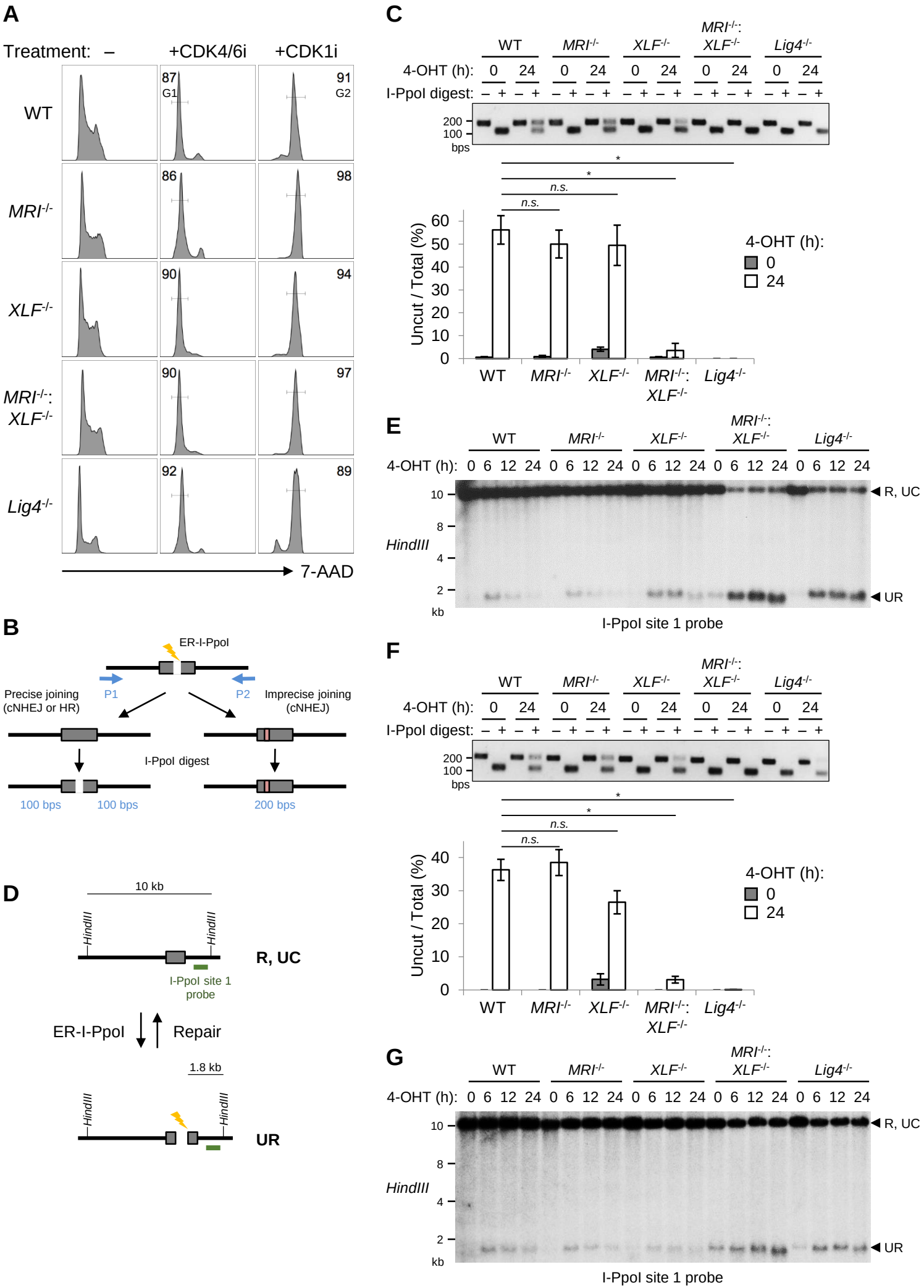
A
Treatment: – +CDK4/6i +CDK1i
WT
MRI-/-
XLF-/-
MRI-/-: XLF-/-
Lig4-/-
87 G1
91 G2
86
98
90
94
90
97
92
89
7-AAD
B
ER-I-PpoI
P1
P2
Precise joining (cNHEJ or HR)
Imprecise joining (cNHEJ)
I-PpoI digest
100 bps
100 bps
200 bps
C
WT MRI-/- XLF-/- MRI-/-: XLF-/- Lig4-/-
4-OHT (h): 0 24 0 24 0 24 0 24 0 24
I-PpoI digest: – + – + – + – + – + – + – + – + – + – +
200
100
bps
*
*
n.s.
n.s.
Uncut / Total (%)
60
50
40
30
20
10
0
4-OHT (h):
0
24
WT MRI-/- XLF-/- MRI-/-: XLF-/- Lig4-/-
D
10 kb
HindIII
HindIII
R, UC
I-PpoI site 1 probe
ER-I-PpoI
Repair
1.8 kb
HindIII
HindIII
UR
E
WT MRI-/- XLF-/- MRI-/-: XLF-/- Lig4-/-
4-OHT (h): 0 6 12 24 0 6 12 24 0 6 12 24 0 6 12 24 0 6 12 24
10
8
4
2
kb
HindIII
R, UC
UR
I-PpoI site 1 probe
F
WT MRI-/- XLF-/- MRI-/-: XLF-/- Lig4-/-
4-OHT (h): 0 24 0 24 0 24 0 24 0 24
I-PpoI digest: – + – + – + – + – + – + – + – + – + – +
200
100
bps
*
*
n.s.
n.s.
Uncut / Total (%)
40
30
20
10
0
4-OHT (h):
0
24
WT MRI-/- XLF-/- MRI-/-: XLF-/- Lig4-/-
G
WT MRI-/- XLF-/- MRI-/-: XLF-/- Lig4-/-
4-OHT (h): 0 6 12 24 0 6 12 24 0 6 12 24 0 6 12 24 0 6 12 24
10
8
4
2
kb
HindIII
R, UC
UR
I-PpoI site 1 probe

Figure S5, related to Figure 3. Combined MRI and XLF deficiency inhibits cNHEJ-mediated repair of I-PpoI DSBs. (A) Flow cytometric analyses of cell cycle phase, as indicated by DNA content (7-AAD), in WT, *MRI*$^{-/-}$, *XLF*$^{-/-}$, *MRI*$^{-/-}$:*XLF*$^{-/-}$, and *Lig4*$^{-/-}$ abl pre-B cells that were untreated (–) or treated with either the CDK4/6 inhibitor palbociclib (CDK4/6i) or the CDK1 inhibitor RO-3306 (CDK1i) for 16 hours. **(B)** Schematic of the I-PpoI DSB repair assay for cNHEJ: PCR amplicons spanning an I-PpoI site (shown as a gray box) were generated from the genomic DNA of abl pre-B cells expressing ER-I-PpoI and digested with I-PpoI to assess the frequency of uncut products containing imprecise junctions formed by cNHEJ. Primers used for PCR are depicted as blue arrows (P1 and P2). The pink box represents a mutation arising from imprecise repair (e.g. a deletion). **(C)** I-PpoI digests of PCR amplicons from ER-I-PpoI-expressing WT, *MRI*$^{-/-}$, *XLF*$^{-/-}$, *MRI*$^{-/-}$:*XLF*$^{-/-}$, and *Lig4*$^{-/-}$ abl pre-B cells arrested in G1 using CDK4/6i prior to treatment with 4-OHT for the indicated lengths of time (hours, h) (top gel). The ratio of the uncut band to the total signal intensity of each lane is quantified (bottom bar graph). Data are mean ± SEM (n = 4). * p <0.05. **(D)** Schematic of the repaired or uncut (R, UC) and the unrepaired (UR) I-PpoI site on mouse chromosome 1 (“site 1”). The locations of the *HindIII* restriction sites and I-PpoI site 1 probe (green line) are shown. **(E)** Southern blot analyses of genomic DNA from G1-phase cells in (C) that were digested with *HindIII* and hybridized to the I-PpoI site 1 probe. Bands corresponding to the R, UC, and UR fragments are indicated. Molecular weights (kilobases, kb) are also shown. **(F)** I-PpoI digests of PCR amplicons from ER-I-PpoI-expressing abl pre-B cells that were arrested in G2 using CDK1i before 4-OHT treatment (top gel) and ratios of the uncut band intensities to the total lane intensities (bottom bar graph) (n = 4). **(G)** Southern blot analyses of genomic DNA from G2-phase cells in (F) that were digested with *HindIII* and hybridized to the I-PpoI site 1 probe.

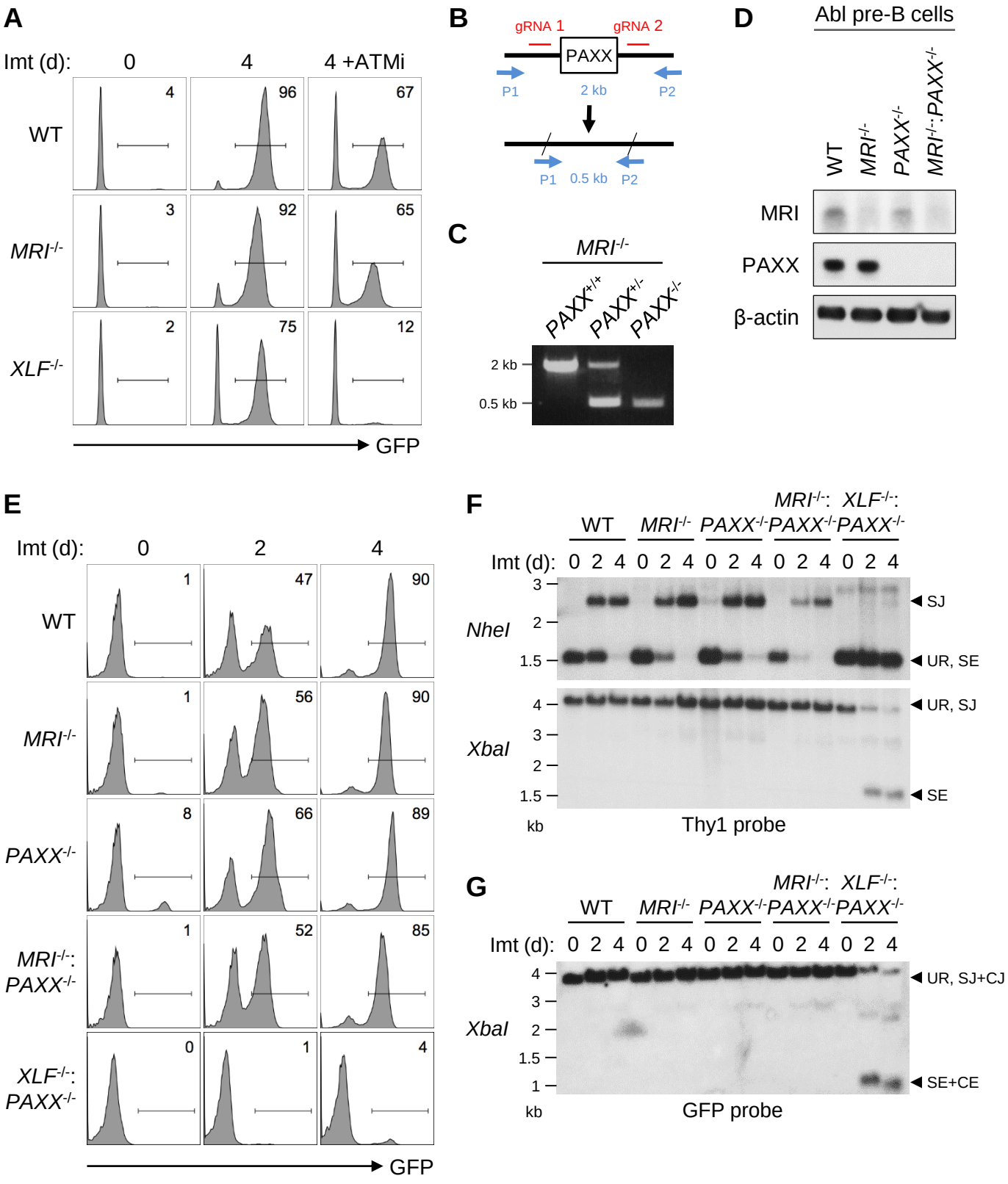
A
Imt (d): 0 4 4 +ATMi
WT
MRI-/-
XLF-/-
4
96
67
3
92
65
2
75
12
GFP
B
gRNA 1
gRNA 2
PAXX
P1
2 kb
P2
P1
0.5 kb
P2
C
MRI-/-
PAXX+/+
PAXX+/-
PAXX-/-
2 kb
0.5 kb
D
Abl pre-B cells
WT
MRI-/-
PAXX-/-
MRI-/-:PAXX-/-
MRI
PAXX
β-actin
E
Imt (d): 0 2 4
WT
MRI-/-
PAXX-/-
MRI-/-: PAXX-/-
XLF-/-: PAXX-/-
1
47
90
1
56
90
8
66
89
1
52
85
0
1
4
GFP
F
MRI-/-: XLF-/-:
WT MRI-/- PAXX-/- PAXX-/- PAXX-/-
Imt (d): 0 2 4 0 2 4 0 2 4 0 2 4 0 2 4
NheI
3
2
1.5
SJ
UR, SE
XbaI
4
3
2
1.5
UR, SJ
SE
kb
Thy1 probe
G
MRI-/-: XLF-/-:
WT MRI-/- PAXX-/- PAXX-/- PAXX-/-
Imt (d): 0 2 4 0 2 4 0 2 4 0 2 4 0 2 4
XbaI
4
3
2
1.5
1
UR, SJ+CJ
SE+CE
kb
GFP probe

Figure S6, related to Figure 3. MRI is not functionally redundant with ATM or PAXX in cNHEJ. (A) Flow cytometric analyses of GFP expression in WT and *MRI*$^{-/-}$ abl pre-B cells that were treated with imatinib in the absence or presence of an ATM kinase inhibitor KU55933 (ATMi) for four days. **(B)** Schematic of the *PAXX* knockout strategy using CRISPR/Cas9 with a pair of gRNAs flanking the entire murine *PAXX* gene. Primers used for screening are depicted as blue arrows (P1 and P2). **(C)** PCR analyses of genomic DNA from *MRI*$^{-/-}$:*PAXX*$^{+/+}$ (parent line), *MRI*$^{-/-}$:*PAXX*$^{+/-}$, and *MRI*$^{-/-}$:*PAXX*$^{-/-}$ abl pre-B cells using primers P1 and P2. **(D)** Western blot analyses of MRI and PAXX in WT, *MRI*$^{-/-}$, *PAXX*$^{-/-}$, and *MRI*$^{-/-}$:*PAXX*$^{-/-}$ abl pre-B cells. β-actin is shown as a protein loading control. **(E)** Flow cytometric analyses of GFP expression in WT, *MRI*$^{-/-}$, *PAXX*$^{-/-}$, *MRI*$^{-/-}$:*PAXX*$^{-/-}$, and *XLF*$^{-/-}$:*PAXX*$^{-/-}$ abl pre-B cells that were treated with imatinib for the indicated lengths of time (days, d). **(F)** Southern blot analyses of genomic DNA from cells in (E) that were digested with *NheI* (top) or *XbaI* (bottom) and hybridized to the Thy1 probe. **(G)** Southern blot analyses of genomic DNA from cells in (E) that were digested with *XbaI* and hybridized to the GFP probe. Bands corresponding to different pMG-INV arrangements are indicated as described in Figure 3. Molecular weights (kilobases, kb) are also shown.

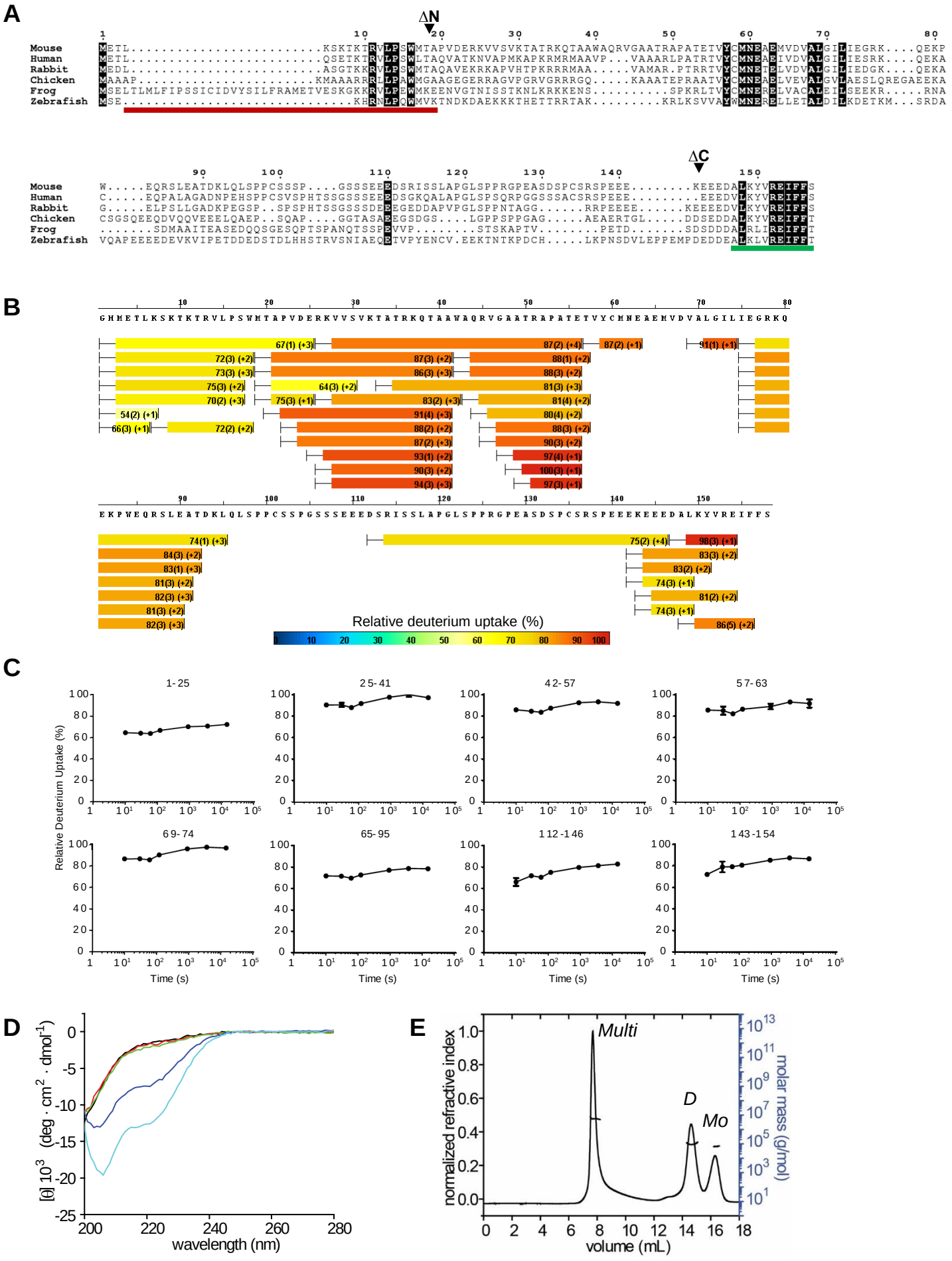
A
ΔN
ΔC
Mouse
Human
Rabbit
Chicken
Frog
Zebrafish
B
Relative deuterium uptake (%)
C
1-25
25-41
42-57
57-63
69-74
65-95
112-146
143-154
Relative Deuterium Uptake (%)
Time (s)
D
[θ] 10^3 (deg · cm^2 · dmol^-1)
wavelength (nm)
E
Multi
D
Mo
normalized refractive index
molar mass (g/mol)
volume (mL)

Figure S7, related to Figure 4. MRI displays structural features of an adaptor. (A) Alignment of the MRI protein sequence across different species. The KBM and XLM are indicated respectively by red and green lines. The black arrows specify the positions of the amino acid truncations in $MRI^{\Delta N}$ and $MRI^{\Delta C}$ (mentioned later in Figure 4). Conserved amino acid residues are shaded in black. **(B)** Hydrogen-deuterium exchange dynamics of MRI. Bars under the amino acid sequence represent the peptide fragments resolved by mass spectrometry. Numbers in each bar indicate the average deuterium percentage over seven incubation times, standard deviation, and peptide charge, respectively. The color code indicates the percentage of average deuterium uptake (see legend). **(C)** Representative deuterium uptake curves for select peptic MRI peptides over seven time points (10, 30, 60, 120, 900, 3600, and 14400 seconds). **(D)** Circular dichroism uptake measurements of the mean residue ellipticity for MRI in the absence (black) or presence of 5% (red), 10% (green), 25% (blue), or 50% (cyan) TFE. **(E)** SEC-MALS analyses reveal that purified MRI elutes as three species: 5,550 ± 16 kDa (multimer, *Multi*), 111 ± 7.8 kDa (dimer, *D*), and 62.1 ± 3.7 kDa (monomer, *Mo*). All data shown are representative of at least three independent experiments.

Table S1, related to Figure 2. Numbers of live births produced from intercrossing *MRI*$^{+/-}$:*XLF*$^{+/-}$ mice.

MRI	*XLF*	Expected	Actual
+/+	+/+	10	9
+/+	+/-	19	22
+/+	-/-	10	10
+/-	+/+	19	30
+/-	+/-	38	34
+/-	-/-	19	15
-/-	+/+	10	14
-/-	+/-	19	20
-/-	-/-	10	0
Total			**154**

Table S2, related to Figure 2. Numbers of mouse embryos from *MRI*$^{-/-}$:*XLF*$^{+/-}$ intercrosses at days E14.5 (top) and E16.5 (bottom).

E14.5			
MRI	*XLF*	Expected	Actual
-/-	+/+	5	7
-/-	+/-	9	7
-/-	-/-	5	5
Total			**19**

E16.5			
MRI	*XLF*	Expected	Actual
-/-	+/+	6	2
-/-	+/-	13	16
-/-	-/-	6	7
Total			**25**

Table S4, related to Key Resources Table. Primer pair sequences used to generate MRI mutant cDNAs for cloning into the pOZ-FH-N retroviral vector.

Construct	Primer Sequences
$MRI^{\Delta N}$	5'-CCCTCGAGATGACCGCGCCGGTGG-3'; 5'-TTGCGGCCGCTCAGCTGAAGAAGATTTCACGA-3'
$MRI^{\Delta C}$	5'-ATGGAAACCCTGAAAAGCAA-3'; 5'-TTGCGGCCGCTCACTTTTCCTCCTCCGGGCTAC-3'
$MRI^{\Delta N\Delta C}$	5'-CCCTCGAGATGACCGCGCCGGTGG-3'; 5'-TTGCGGCCGCTCACTTTTCCTCCTCCGGGCTAC-3'